Evaporation–Wind Feedback and the Organizing of Tropical Convection on the Planetary Scale. Part I: Quasi-Linear Instability

SHANG-PING XIE

Department of Geophysics, Tohoku University, Sendai, Japan

ATSUSHI KUBOKAWA

Department of Earth System Science and Technology, Kyushu University, Kasuga, Japan

KIMIO HANAWA

Department of Geophysics, Tohoku University, Sendai, Japan

(Manuscript received 5 February 1992, in final form 19 April 1993)

ABSTRACT

Recent GCM experiments have suggested the existence of a zonal wavenumber one convective mode in the aqua-planet atmosphere. This paper reports that a planetary-scale mode can be generated in a very simple reduced gravity model that is linear except for two nonlinearities in its cumulus parameterization: conditional heating and wind speed–dependent surface evaporation. The behavior of the model solution is shown to be independent of the perturbation amplitude so that a constant growth rate can be defined. This amplitude-independent nonlinear system is here called the quasi-linear (QL) system.

An instability is found in a moist stable atmosphere at rest, which is stable in existing theories. A global integral theorem confirms the existence of the QL instability. The instability has an equatorially trapped, zonal wavenumber one structure, growing exponentially and propagating eastward at a speed close to that of the neutral, linear moist Kelvin wave. A new type of evaporation–wind feedback (EWFB) is responsible for the instability, which does not require the existence of mean easterlies and arises from an in-phase relation between temperature perturbation and condensational heating directly due to surface evaporation. By performing calculations in zonally periodic spherical triangles of various zonal sizes, an increasing relation between the growth rate and the zonal size of the domain is found, which explains why the wavenumber one mode is selected.

The instability has several observed features of the Madden–Julian oscillations, including the slow eastward propagation and wavenumber one structure. Its phase speed, growth rate, and spatial structure are insensitive to model resolution, suggesting its relevance to the planetary-scale modes reported in aqua-planet GCMs.

1. Introduction

Latent heating in deep convection is the main energy source of atmospheric motion in the tropics. Instead of being homogeneous over regions of high SST (sea surface temperature), tropical convection shows highly organized order. On the planetary scale, they often gather into a single cluster that has a zonal size of a few thousand kilometers and propagates eastward (Knutson and Weickmann 1987). The organization of tropical convection on the planetary scale has long been considered as the source of the tropical intraseasonal oscillations (ISO) (Madden and Julian 1972). This viewpoint is also supported by recent GCM (general circulation model) experiments under realistic (Lau and Lau 1986; Hayashi and Golder 1986, 1988) and idealized zonally symmetric aqua-planet (Hayashi and Sumi 1986; Swinbank et al. 1988; Lau et al. 1988; Tokioka et al. 1988) conditions. Although these GCMs have different physical parameterizations, different vertical and horizontal resolutions, and different mesoscale convection from model to model, zonal wavenumber one structures were found in the geopotential, zonal wind velocity, and sometimes precipitation fields. This suggests that a planetary-scale mode of tropical convective motion exists.

Searching for this mode with simple theoretical models has been attempted by many investigators. Among the proposed theories is the wave–CISK (conditional instability of the second kind) theory. In coarse-resolution models, convection generated by the wave–CISK has been shown to organize into a zonal wavenumber one structure when conditional heating is incorporated (Lau and Peng 1987; Hendon 1988, among many others). On the other hand, the wave–CISK is also known to increase its growth rate with the

Corresponding author address: Dr. Shang-Ping Xie, Joint Institute for the Study of the Atmosphere and Ocean, University of Washington, GJ-40, Seattle, WA 98195.

decrease of ascending area (Kuo 1961; Dunkerton and Crum 1991). Since the zonal scale of an instability decreases proportionally with increasing growth rate, fast growing wave–CISK favors very small zonal scales and does not necessarily choose the wavenumber one mode. In a high-resolution model, Xie (1991) found a high wavenumber wave–CISK mode with multiple east–west circulation cells that are of similar strength and nearly equally spaced along the equator.

Precipitation in a wave–CISK model is caused by gathering ambient existing moisture. Since the mean residence time of water vapor in the atmosphere is one week to ten days, surface evaporation, which supplies the moisture, could be important for the slow motion like the ISO with a time scale longer than ten days. In some GCMs, surface evaporation was found to be important in maintaining the wavenumber one structure of the model ISO. When the wind speed dependence was removed from the surface evaporation formula, the eastward-propagating wavenumber one mode significantly reduced its amplitude (Neelin et al. 1987) or became invisible (Numaguti and Hayashi 1991).

The first theories taking into account the effect of surface evaporation were proposed by Emanuel (1987) and Neelin et al. (1987). They showed that in the presence of surface easterlies the Kelvin wave was destabilized by so-called evaporation–wind feedback (EWFB). However, in their linear theories the unstable Kelvin wave increases its growth rate with the wavenumber, and hence does not explain why the wavenumber one mode is dominant in the real atmosphere and GCMs. Moist convection in the real atmosphere is highly nonlinear. Kuo-type cumulus parameterization requires that precipitation in an air column be equal to horizontal moisture convergence plus surface evaporation, which in a two-level model may be expressed as

$$Q = \begin{cases} q\nabla\cdot\mathbf{u} + C'_E\Delta q|\mathbf{u}|, & \text{if} \quad \nabla\cdot\mathbf{u} \geqslant 0 \\ 0, & \text{otherwise,} \end{cases} \tag{1.1}$$

where Q is latent heating, $-\mathbf{u}$ the low-level wind velocity, C'_E is the evaporation coefficient, and q and $-\Delta q$ are surface humidity and its difference from the saturated value. Two nonlinear terms appear in (1.1). Moist convection is characterized by conditional heating that cannot be linearized irrespective of perturbation's amplitude. The absolute value nonlinearity can be linearized only if there are mean surface winds in the basic state and the perturbation winds are weak.

In Part I of this two-part paper, we study the stability problem using the full form of (1.1). The basic state is assumed to be at rest with zero surface wind ($U_0 = 0$). We assume that the mean surface easterlies are not the condition for the organization of convection. In fact, surface winds are observed to be weak or even westerly in the Indian and western Pacific oceans where the ISO has maximum amplitude (Wang 1988). This assumption puts no restriction on the amplitude of perturbation. To avoid the wave–CISK flow regime, we confine most of our discussion to the stable regime of wave–CISK. With these parameter values, both wave–CISK and linear EWFB theories predict a stable atmosphere. The stability problem in this parameter regime is of great theoretical interest, since it raises a fundamental question of whether a resting atmosphere stable to the wave–CISK is really stable. It is also of practical significance since recent observations reveal that the tropical atmosphere is marginally stable (Xu and Emanuel 1989). We will show that a new nonlinear instability exists, which propagates eastward and favors the growth of a wavenumber one mode.

The model equations are described in section 2. In section 3, the spatial structure and unstable mechanism of the instability are described with the simplest single-baroclinic-mode model. The effect of surface evaporation on the wave–CISK is discussed in section 4. In section 5, we generalize our discussion in a two-baroclinic-mode model. Concluding remarks are given in section 6. Section 2 is given for completeness; the reader may wish to skip to section 3.

2. Model equations

In a continuously stratified atmosphere where cumulus heating excites only the first two baroclinic modes, the equations that govern small amplitude motion are

$$(\mathbf{u}_j)_t + f\mathbf{k}\times\mathbf{u}_j = -\nabla\varphi_j, \tag{2.1}$$

$$(\varphi_j)_t + C_j^2\nabla\cdot\mathbf{u}_j = C_1^2\frac{f_j}{j}Q, \tag{2.2}$$

$$Q = [q(\nabla\cdot\mathbf{u}_1 + d_2\nabla\cdot\mathbf{u}_2) + C'_E\Delta q|\mathbf{u}_1 + \mathbf{u}_2|] \times H(\nabla\cdot\mathbf{u}_1 - \nabla\cdot\mathbf{u}_2/\sqrt{2}), \tag{2.3}$$

where H is the Heaviside step function defined as

$$H(D) = \begin{cases} 1, & \text{if} \quad D \geqslant 0, \\ 0, & \text{otherwise,} \end{cases} \tag{2.4}$$

subscript j ($j = 1, 2$) denotes jth baroclinic mode, $C_j = S/(j\pi)$ is the phase speed of jth long gravity wave mode in an atmosphere with constant static stability S, φ the geopotential, d_2 the efficiency of the second mode in producing low-level moisture convergence. Further, $f_1 \equiv 1$ and f_2 denotes heating partition ratio between the two modes or the height of heating profile; a larger value of f_2 means that maximum heating occurs at a higher height. Surface humidity q is so normalized that in the single-mode model ($f_2 = 0$), the moist static stability becomes zero at $q = 1$ and the wave–CISK occurs when $q > 1$. Details in deriving (2.1)–(2.4) may be found in Xie (1991).

There seems to be no consensus in the definition of the wave–CISK. We define wave–CISK to be the in-

stability in the absence of surface evaporation. As will be seen, there are other instabilities in (2.1)–(2.4) not due to conditionally unstable stratification. By this definition, the propagating wave–CISK occurs if

$$\frac{3}{(2+\sqrt{F})^2} < q < \frac{3}{(2-\sqrt{F})^2}, \text{ and } F > 0, \quad (2.5)$$

where $F = 2d_2f_2$ (Xie 1991). The stationary wave–CISK occurs if

$$q > \frac{1}{1-F}, \quad \text{for} \quad F < \frac{1}{4} \quad \text{and}$$

$$q > \frac{3}{(2-\sqrt{F})^2} \quad \text{for} \quad F > \frac{1}{4}. \quad (2.6)$$

Equations (2.1)–(2.2) are linear but (2.3) contains two nonlinear functions; the magnitude of the wind velocity and the Heaviside function representing conditional heating. Although (2.3) cannot be linearized, it is obvious that if u is a solution of (2.1)–(2.3), $A \cdot u$ is a solution, too, where A is an arbitrary positive constant. Namely, the behavior of (2.1)–(2.3)'s solution is independent of solution's amplitude. To distinguish it from the nonlinear equations with quadratic terms, we call this amplitude-independent nonlinear system the quasi-linear (QL) system hereafter. As we will see, an exponentially growing solution is possible in a QL system and a constant growth rate can be defined.

We choose $C_1 = 43$ m s^{-1}, $d_2 = 0.45$, and $C'_E = 5.2 \times 10^{-7}$ m^{-1}, as in Xie (1991). We use $\Delta q = 0.2$ unless otherwise specified. Equations (2.1) and (2.2) are two sets of shallow-water equations, which are solved using the spectral method in the global domain. Bourke (1988) gives a detailed description of the spectral method. Harmonic diffusion terms are added to (2.1)–(2.2) with a coefficient of 2.5×10^5 m^2 s^{-1}. A semi-implicit time stepping scheme is employed. Time steps are taken to be 60 minutes in the R15 and R31 models, 30 minutes in the R63, and 15 minutes in the R127 model.

3. Eastward-propagating mode

In this and the next sections, we first consider the simple single-baroclinic-mode model and set $f_2 = 0$. Dropping the subscript $j = 1$, (2.1)–(2.3) are simplified to

$$\mathbf{u}_t + f\mathbf{k} \times \mathbf{u} = -\nabla\varphi, \quad (3.1)$$

$$\varphi_t + C_1^2 \nabla \cdot \mathbf{u} = C_1^2 Q, \quad (3.2)$$

$$Q = (q\nabla \cdot \mathbf{u} + C'_E \Delta q |\mathbf{u}|) \cdot H(\nabla \cdot \mathbf{u}). \quad (3.3)$$

This single-mode model of the continuously stratified atmosphere is equivalent to the vertically discrete two-level model, where the midlevel potential temperature $\bar{\theta}$ is related to the upper- to low-level geopotential difference by $\bar{\theta} = \varphi / c_p B$, where $c_p B = 124$ J K^{-1} kg^{-1}. An alternative derivation for (3.3) can be found in Part II.

We have introduced deep upward motion as the condition for deep convection. Only when deep upward motion occurs can low-level moist air be lifted to an upper level where it becomes saturated, causing precipitation and deep convection. In regions of weak downward motion, we assume that the local moisture gain, if there is any, is used to increase the low-level moisture mixing ratio rather than to produce deep convection. Using deep upward motion as the criterion for deep convection is consistent with composite analysis of the ISO in GCMs (Lau et al. 1988; Numaguti and Hayashi 1991). In the GFDL GCM, Hayashi and Golder (1993) found that precipitation is almost always associated with upward motion at low level. Considering the uncertainty in condition for large-scale deep convection, we have conducted experiments replacing $H(\nabla \cdot \mathbf{u})$ in (3.3) with $H(q\nabla \cdot \mathbf{u} + C'_E \Delta q |\mathbf{u}|)$ and found that this did not yield any qualitative change in the results we will discuss.

A stationary wave–CISK occurs with $q > 1$. In a two-level model, $q = 1$ corresponds to a mixing ratio at the surface of 2×10^{-2} (see Part II). To avoid the wave–CISK, we choose $q = 0.9$ in this section. Since the stratification is stable and there are no mean zonal winds, neither the wave–CISK nor linear EWFB theories predict an instability. When an equatorial Kelvin wave with a single ascending area is put into this quasi-linear system as the initial perturbation, however, Fig. 1 shows that the perturbation grows exponentially, propagating eastward. The period and e-folding time of the growth rate are estimated to be 31 and 4.1 days, respectively. The corresponding phase speed is 14.9 m s^{-1}, very close to the linear moist Kelvin wave's phase speed $c = C_1(1-q)^{1/2} = 13.6$ m s^{-1} but much slower than that of the dry wave. Hereafter, we call this eastward-propagating, unstable mode the QL E mode or simply the E mode. Figure 2 shows the spatial structure of the E mode. The significant cumulus heating is only confined to the equator and the flow field resembles the so-called Gill pattern with the Kelvin wave response east of the heating and the Rossby one west. Although we have not prescribed any external wind in the basic state, a zonal-mean Hadley circulation is generated by the zonal-mean cumulus heating and the easterly trades prevail in the tropics. Even at the equator, weak zonal-mean surface easterlies are found because of the momentum diffusion. Unlike the linear EWFB Kelvin mode, the unstable growth of the E mode, however, is not due to the zonal-mean easterlies. In an experiment where the zonal-mean winds are artificially removed in calculating evaporation, an eastward-propagating instability with similar phase speed, growth rate, and spatial structure develops. In the rest of the section, we discuss the unstable mechanism of the E mode.

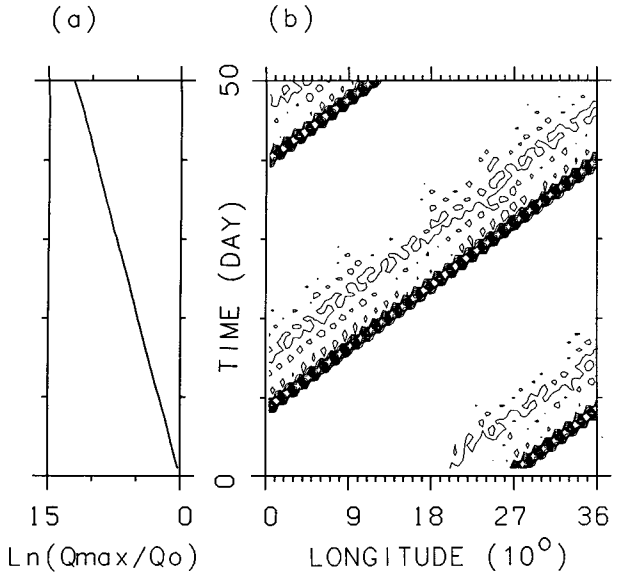

FIG. 1. (a) Amplitude of the E mode in an R31 model as the function of time. The horizontal axis is in logarithm so that the slope of the curve gives the growth rate. (b) Time–longitude section along the equator of latent heating rate normalized by instantaneous maximum at each time. Contour intervals are 0.1 and the zero contour is omitted.

In a QL system, a solution exists with an unchanging structure that propagates at a constant speed c_r and grows at a constant rate σ_i

$$\begin{Bmatrix} \mathbf{u} \\ \varphi \\ Q \end{Bmatrix} = \begin{Bmatrix} \mathbf{U}(x - c_r t, y) \\ \phi(x - c_r t, y) \\ Q^*(x - c_r t, y)/C_1^2 \end{Bmatrix} e^{\sigma_i t}. \quad (3.4)$$

Substitution of (3.4) in (3.1)–(3.3) yields equations that determine the spatial structure of the solution in the moving coordinate $X = x - c_r t$,

$$-c_r \frac{\partial \mathbf{U}}{\partial X} + f\mathbf{k} \times \mathbf{U} = -\nabla\phi - \sigma_i \mathbf{U}, \quad (3.5)$$

$$-c_r \frac{\partial \phi}{\partial X} + C_1^2 \nabla \cdot \mathbf{U} = Q^* - \sigma_i \phi, \quad (3.6)$$

which are the same as the equations for the problem of the steady response to a heat source moving at the phase speed of the instability. In this steady response problem the dissipation rate equals the growth rate in the instability problem. Under the long-wave approximation, (3.5)–(3.6) can be simplified into a set of amplitude equations for the Kelvin and long nondispersive Rossby waves as in Gill (1980) except that Doppler-shifted phase speeds,

$$c_K = C_1 - c_r, \quad \text{for the Kelvin wave,} \quad (3.7)$$

$$c_R^{(n)} = -\left(c_r + \frac{C_1}{2n+1}\right), \quad \text{for the } n\text{th Rossby wave,} \quad (3.8)$$

should be used. To an eastward-moving heating, the Kelvin wave response is enhanced while the Rossby ones are suppressed compared to the case of a standing heating, since the Kelvin wave with a reduced phase speed stays longer in the heating area and receives more energy to reach larger amplitude.

Figure 3a gives a close look at the mode structure at the equator. Leading the convective region is a sharp precipitation peak. Following it is a long precipitation tail. The surface easterlies east of the heating peak are much stronger in magnitude than the westerlies west, indicating an enhanced Kelvin response. This is partly due to the eastward propagation of the instability. In a coordinate system moving at the phase speed of the instability, the Doppler-shifted phase speed of the Kelvin wave is nearly equal to that of the first Rossby wave mode, while their ratio is three in a stationary coordinate. Also responsible for the strong easterlies is the superposition or accumulation of the Kelvin waves generated by the precipitation tail to the west. Since the stratification is stable, the part of the latent heating associated with horizontal moisture convergence, though much larger than the surface evaporation, is overwhelmed by adiabatic cooling and cannot cause

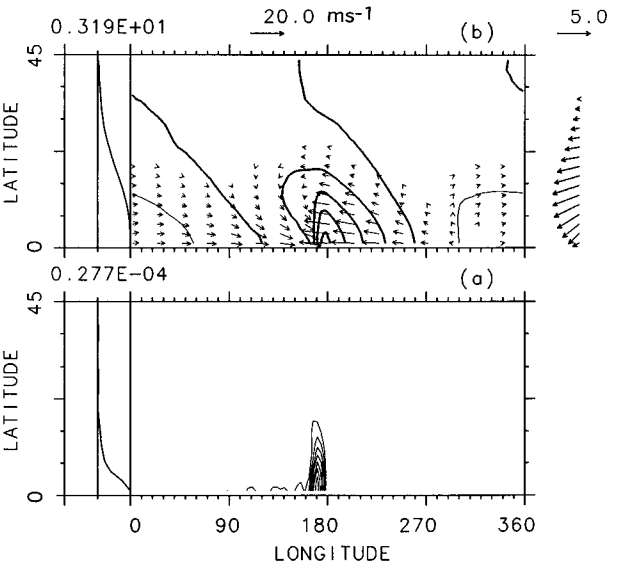

FIG. 2. Horizontal structure of the E mode in an R31 model: (a) cumulus heating rate with interval of 5×10^{-5} K s^{-1} and zero contour omitted, (b) potential temperature at the midlevel with interval of 1 K and low-level wind velocity vector with the scale shown. Meridional distribution of the zonal mean of the contoured variable is shown on the left with the numeral denoting the maximum, and that of the vector variable on the right with the scale shown above. Only the deviation from the zonal mean is shown in (b). The meridional coordinate has a scale four times as large as the longitudinal one.

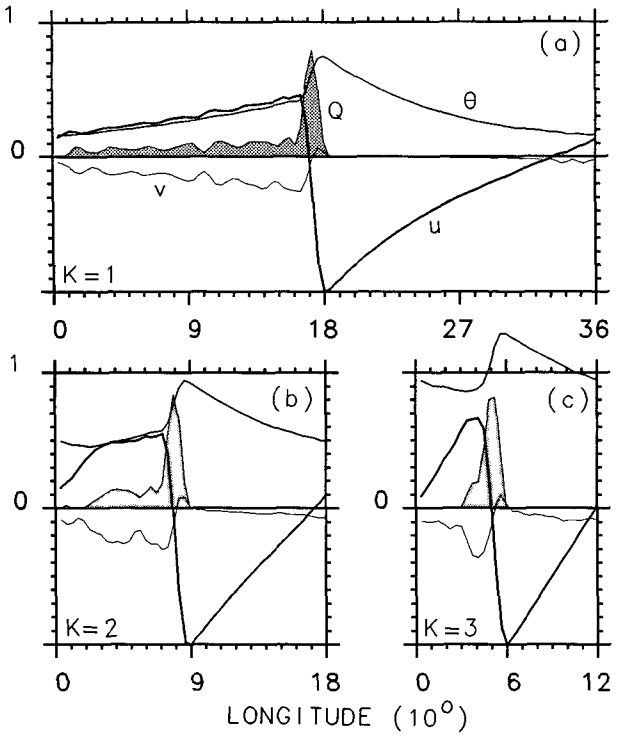

FIG. 3. Zonal structure of the E mode at the equator in an R31 model with (a) $K = 1$, (b) $K = 2$, and (c) $K = 3$. Units for the zonal and meridional components of the wind velocity, midlevel potential temperature, and cumulus heating (hatched) are 20 m s^{-1}, 2 m s^{-1}, 10 K, and 5×10^{-4} K s^{-1}, respectively. Meridional velocity at the first Gaussian grid north of the equator is plotted.

an instability. Surface evaporation is responsible for the unstable growth, as is evident from the global integral theorem (A.6). Even without knowledge of the phase relation between the wind speed and temperature (or geopotential), (A.6) predicts the destabilization of the E mode since its temperature perturbation is everywhere positive. The in-phase relation between the wind speed (evaporation) and temperature in Fig. 3a enhances the instability. The slight phase lead of the wind speed tends to accelerate the propagation of the instability, making its phase speed a little faster than that of the linear neutral moist mode.

Although the zonal wavenumber one mode is dominant in the global calculation domain, model equations may have other zonally periodic solutions with higher zonal wavenumber. We have obtained such solutions by carrying out calculations in zonally periodic spherical triangles $0 \leq \theta \leq 90°$, $0 \leq \lambda \leq 360°/K$, $K = 1, 2, 3$, where θ and λ denote latitude and longitude, respectively. The phase speed does not change in all the calculations, while the growth rate of the E mode increases with the zonal extent of the domain (Table 1). The growth rate decreases about 15% when the globe is divided into twin spherical triangles. Figure 3 shows how the spatial structure of the E mode changes with K. The long precipitation tail in the case of $K = 1$ shortens with $K \geq 2$. This reduces the Kelvin wave response. Reduction in the domain's size also causes Kelvin and Rossby wave responses to interfere. In fact, the e-folding zonal scale of a Kelvin wave is about 180°, which is comparable with or larger than the domain's size if $K \geq 2$. Both effects above tend to reduce wind speed difference across the heating peak and therefore the east–west asymmetry in surface evaporation, leading to the decrease in the growth rate. The proportional relation between the growth rate and zonal extent of the domain thus explains why the E mode instability always selects the mode with a dominant wavenumber one structure, the largest scale the earth allows. In an experiment where the $K = 2$ mode was used to initiate the calculation in the global domain, the $K = 1$ mode becomes dominant in 80 days (not shown), supporting the above argument of the scale selection.

As Xie (1991) showed, the growth rate and dominant spatial scale of the wave–CISK strongly depends on the horizontal resolution of the model. We have run our QL-EWFB model with various resolutions to test the sensitivity. The change in the phase speed is negligible (not shown). Table 1 shows that the growth rate of the E mode is insensitive to the model resolution. So are its zonal structures, which are shown in Fig. 4. The structures of the E mode are identical in the R63 and R127 models. The difference in the meridional wind arises from the fact that the most equatorward grid of the R127 model is closer to the equator than the R63 model's. Even the coarse-resolution R15 model works very well in simulating the E mode. Since its phase speed, growth rate, and spatial structure are all insensitive to the model resolution, the planetary-scale E mode is a solution to the model differential equations (3.1)–(3.3).

Figure 5 shows the dependence of the phase speed and growth rate on the value of Δq, which helps us to trace the origin of the E mode. The growth rate decreases rapidly with Δq while the phase speed almost does not change, remaining close to the linear moist value. With $\Delta q = 0$, which is equivalent to eliminating the evaporation term, there is no growing mode and the dominant phase speed cannot be determined numerically because of the existence of various types of

TABLE 1. Dependence of the e-folding growing time (unit: day) of the quasi-linear E mode on the zonal size of the domain (line) and on the horizontal resolution of the model (column).

	K		
	1	2	3
R63	4.16	4.76	5.83
R31	4.15	4.76	5.89
R15	4.29	5.63	—

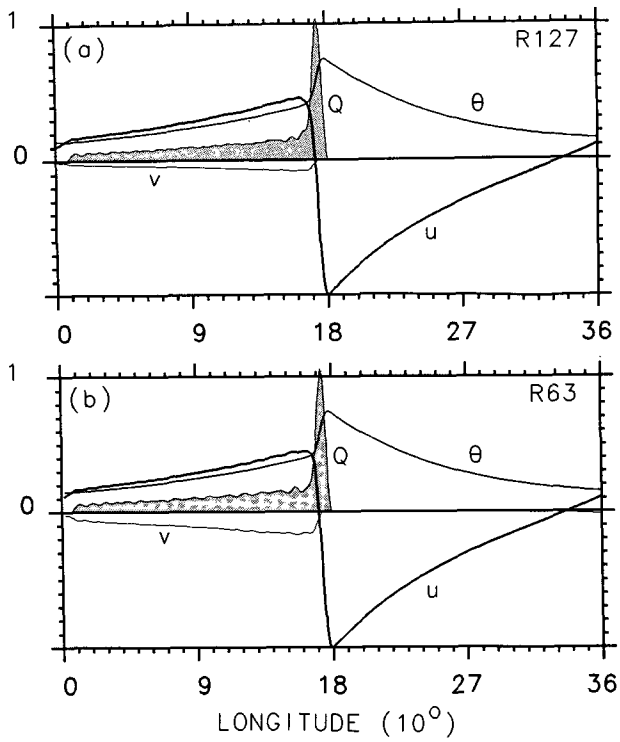

FIG. 4. Same as Fig. 3a but in (a) R127 and (b) R63 models.

waves. Therefore, this confirms that surface evaporation causes the E mode instability.

Figure 6 shows the dependence of the phase speed and growth rate on q. The phase speeds of the E mode and linear moist Kelvin wave coincide almost everywhere except at $q \approx 1$ where the latter approaches zero. Although the phase speed of the E mode for small q is slightly smaller than that of the linear moist Kelvin wave in Fig. 6a, this possibly arises from the implicit time stepping scheme, which tends to slow down the wave's phase speed. The growth rate is a monotonously increasing function of q, suggesting that active convection occurs over high sea surface temperature.

In our calculation, the E mode is the only instability in the parameter regime of $q < 1$, where, irrespective of initial condition, the wavenumber one E mode becomes domianant finally. For q > 1, however, we cannot obtain an E mode solution. Instead, the wave–CISK is dominant, as will be shown next.

4. Westward-propagating mode

If we choose the gravest Rossby wave to initiate the calculation, with $q = 1.0$, Fig. 7 shows that a westward-propagating, exponentially growing instability (W-mode) develops although the linear theory predicts a marginally stable atmosphere. The period and e-folding time are estimated to be 53 and 2.3 days, respectively, in an R31 model. The W mode involves an intensive convection that is confined to a small equatorial area in both zonal and meridional directions (Fig. 8). In the flow field, the Rossby response is dominant. Figure 9 shows the zonal structure of the W mode at the equator. The surface westerlies west of the precipitation peak are much stronger than the easterlies to the east, in contrast to the case of E mode. Enhanced surface westerlies are a characteristic of the steady Gill pattern in response to a stationary isolated heating. With $q = 1$, latent heating associated with horizontal moisture convergence is compensated by adiabatic cooling and has no net effect on temperature change in the convective region. The phase relation between surface evaporation and temperature determines the propagating and growing characters of the W mode. The westward phase shift of the peak in surface westerly from that in the temperature causes the whole structure to move westward. At the same time, since surface westerly winds are almost in phase with the temperature, they reinforce each other through the evaporation term, destabilizing the disturbance.

Figure 6 also shows the dependence of the W mode growth rate on the surface humidity in the R15 model. In contrast to the E mode, the existence of the W mode strongly depends on the stratification or the value of q. We could not obtain a W mode for $q \leq 0.95$. The

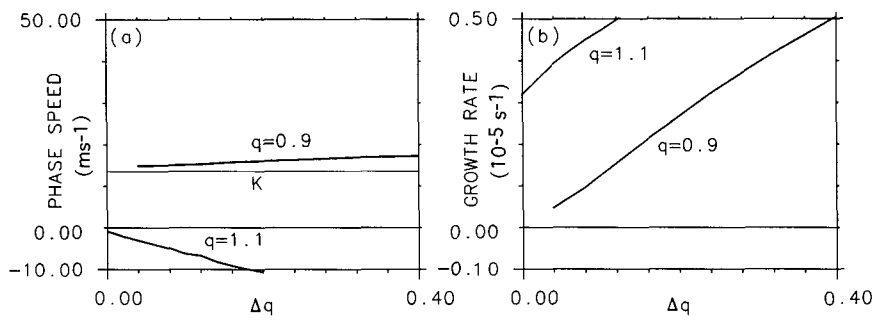

FIG. 5. Dependence on Δq in the R15 model of (a) phase speeds and (b) growth rates of the E mode with $q = 0.9$ and the W mode with $q = 1.1$. The thin line marked with K in (a) indicates the phase speed of the neutral, linear moist Kelvin wave, $c = C_1\sqrt{1-q}$.

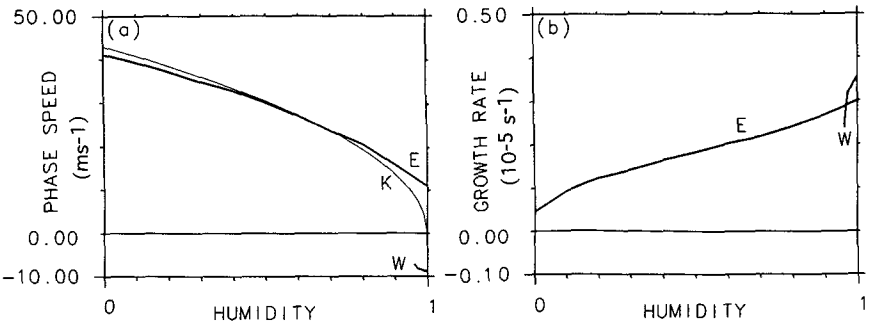

FIG. 6. Dependence on the surface humidity q in the R15 model of (a) phase speed and (b) growth rate with $\Delta q = 0.2$. The thin curve in (a) is for the neutral, linear moist Kelvin wave (K).

growth rate of the W mode is also very sensitive to the model's resolution, whose e-folding time at $q = 1.0$ decreases from 3.3 days in the R15 model to 2.3 days in the R31 model. So is the spatial structure; compared with that in Fig. 8, the convective area in the R15 model is much broader (not shown). Furthermore, the model resolution also affects the parameter range where the W mode exists, which shrinks from $q > 0.95$ in the R15 to $q > 0.96$ in the R31 model. This seems to suggest that the W mode with $q < 1$ is only a spurious solution of the low-resolution numerical model. Implicit time differencing may be responsible for the existence of the W mode in $q < 1.0$, which distorts the wave speed and may change the unstable condition for the wave–CISK in the numerical model.

The westward-propagating instability is the only dominant mode for $q > 1.0$. The dependence on Δq of the phase speed and growth rate of the W mode is shown in Fig. 5 with $q = 1.1$. With the resolution of R15, large value of Δq yields a large growth rate. Unlike the E mode, however, the properties of the W mode are sensitive to the model resolution. Generally, the size ratio of the evaporation term to moisture convergence term is dependent on the size of ascending area L, that is,

$$o\left(\frac{C'_E \Delta q |\mathbf{u}|}{q \nabla \cdot \mathbf{u}}\right) = \left(\frac{C'_E \Delta q}{q}\right) \frac{1}{L}, \qquad (4.1)$$

which states that the smaller the ascending area, the less important the evaporation becomes. Since the ascending area of a wave–CISK mode tends to contract infinitely (Kuo 1961; Dunkerton and Crum 1991), the evaporation term is negligibly small in the unstable parameter regime of the wave–CISK. Therefore, the westward-propagating W mode is nothing but a virtual image of the wave–CISK solution in the low-resolution model, which is expected to become stationary and

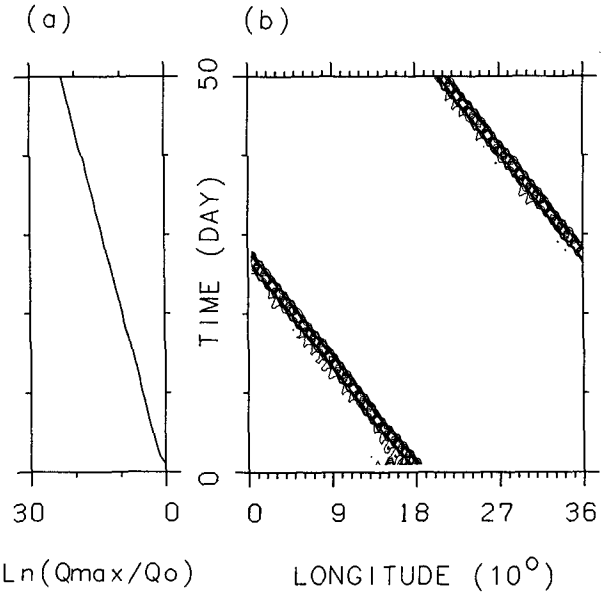

FIG. 7. Same as Fig. 1 but for the W mode with $q = 1$.

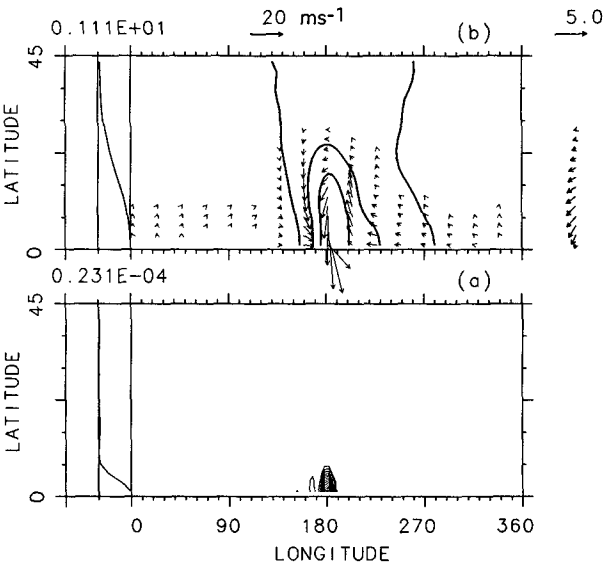

FIG. 8. Same as Fig. 2 but for W mode with $q = 1$.

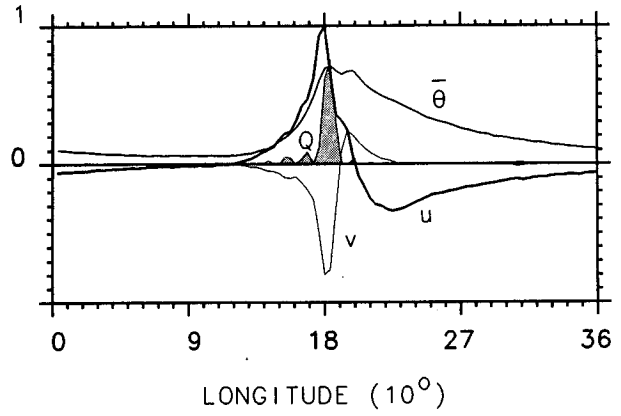

FIG. 9. Same as Fig. 3a but for W mode with $q = 1$. Units for the zonal and meridional components of the wind velocity, midlevel potential temperature, and cumulus heating are 20 m s^{-1}, 5 m s^{-1}, 5 K, and 1×10^{-3} K s^{-1}, respectively.

lose preferred planetary scale when the resolution is increased. The slowing down of the phase speed of the W mode for $q > 1$ was observed when the model resolution was increased from R15 to R31 (not shown).

5. Quasi-linear EWFB mode in a two-mode model

In this section, we investigate the effect of a change in the vertical heating profile on the convective instabilities. Since the first baroclinic mode is observed to be dominant in the tropics, we adopt the simple two-baroclinic-mode model described in section 2. An R15 version is used. The following solutions, obtained by time integration, are the fastest growing modes but are not necessarily the only ones.

First, we consider a deep heating profile with $f_2 = 0.1$. According to the linear analysis [see (2.5)–(2.6)], the propagating and stationary wave–CISKs occur with $0.57 < q < 1.04$ and with $q > 1.10$, respectively. In the stable region of the wave–CISK $q < 0.57$, the inclusion of the surface evaporation term yields an eastward-propagating EWFB instability, whose phase speed and growth rate are shown in Fig. 10. We found that the phase speed of the EWFB mode is very close to that of the linear moist Kelvin wave. The growth rate increases with q and is close to but slightly larger than that of its counterpart in the single-mode model. The zonal structure of the EWFB mode is depicted in Fig. 11a, which resembles that of the single-mode model. The second baroclinic mode has an amplitude much smaller than the first mode and is excited only west of the precipitation front since the instability propagates faster than the second-mode Kelvin wave. With $q < 0.57$, no significant change was observed in the phase speed, growth rate, and spatial structure when a higher-resolution R31 model was used, indicating that the R15 model has captured the solution of the differential model equations. In the unstable regime of the wave–CISK $q > 0.57$, however, the growth rate and spatial structure of the numerical solution strongly depend on the horizontal resolution, as expected from the discussion at the end of section 4.

With $f_2 = -0.1$, the linear theory predicts a stationary wave–CISK when $q > 0.92$. In the stable regime of the wave–CISK, the phase speed of the EWFB mode is close to that of the neutral, linear moist wave solution in the absence of surface evaporation. The model has two solutions with high and low phase speeds. At about $q = 0.6$ the fastest growing mode jumps from the high phase speed solution to the low phase speed one, as seen in Fig. 10a. The horizontal structure of the mode with $q < 0.6$ resembles that with $f_2 = 0.1$ except for a phase reversal in the second mode (Fig. 11b). The growth rate for $q < 0.6$ is smaller than those for $f_2 = 0$ and $f_2 = 0.1$ for small q. This dependence of the growth rate on f_2 seems to be due to the zonal phase difference between the two baroclinic modes but not to the modification of surface evaporation by the second mode. This increasing relation between σ_i and f_2 does not change when the effect of the second mode on surface evaporation is artificially suppressed (not shown). After the mode jumps to a phase speed smaller than that of the second-mode Kelvin wave for $q > 0.6$, its spatial structure drastically changes (Fig. 11c). Because the second-mode Kelvin wave can propagate eastward at a reduced speed, its amplitude is greatly enhanced. Since the second-mode Kelvin wave response is in phase with that of the first mode at the surface, it

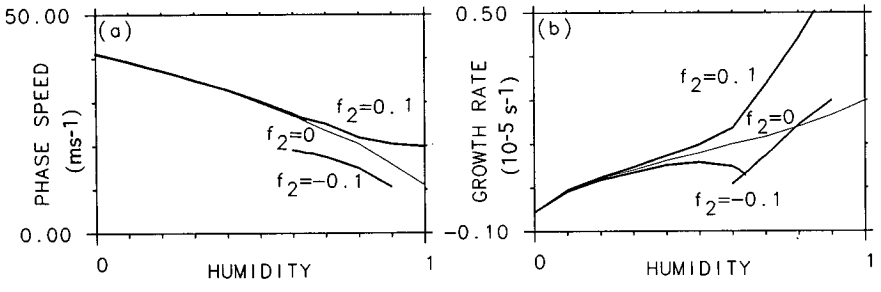

FIG. 10. Same as Fig. 6 except in a two-mode model with $f_2 = -0.1$ and 0.1. Curves for $f_2 = 0$ are plotted thin.

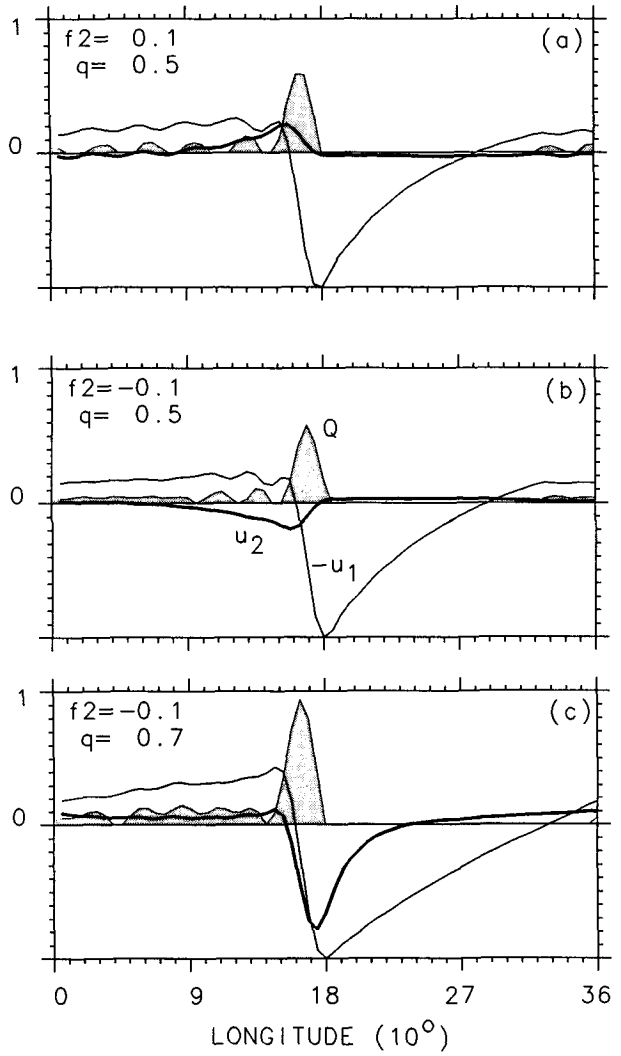

FIG. 11. Same as Fig. 3a but in an R15 model with (a) $f_2 = 0.1$ and $q = 0.5$, (b) $f_2 = -0.1$ and $q = 0.5$, and (c) $f_2 = -0.1$ and $q = 0.7$. Only zonal velocities of the first (thin) and second (thick) baroclinic modes at the surface are shown. Units for velocities associated with the first and second modes and cumulus heating are 20 m s^{-1}, 10 m s^{-1}, and 2×10^{-4} K s^{-1}, respectively.

strengthens the zonal variation in the evaporation, acting to enhance the unstable growth. In fact, the growth rate of the $f_2 = -0.1$ mode exceeds that of the $f_2 = 0$ for large q. The coexistence of two modes at $q = 0.64$ is of special interest; although having the same heating profile and growth rate, they are of different vertical structure and phase speed.

The wave–CISK owes its existence to the temperature stratification and vertical heating profile. The EWFB instability does not; it exists in and dominates the stable parameter regime of the wave–CISK.

6. Discussion

The stability of the moist atmosphere has been investigated in an amplitude-independent nonlinear (or quasi-linear) model described by linear reduced gravity equations forced by nonlinear cumulus heating. The atmosphere is stable to the wave–CISK and is at rest, without any mean flow, but is destabilized by the inclusion of wind speed–dependent surface evaporation. An equatorially trapped instability with a zonal wavenumber one structure was generated. It propagates eastward at a speed close to that of the linear moist Kelvin wave. An evaporation–wind feedback, generated by an in-phase relation between surface wind speed and vertical mean temperature, is responsible for the unstable growth. By dividing the earth into zonally periodic spherical triangles, the instability growth rate is found to be proportional to the zonal size of the triangle. As a result, the wavenumber one E mode, with the largest zonal scale the earth allows, is always selected to prevail in the global domain. The EWFB instability and wave–CISK are two different solutions to the same model equations and they dominate different parameter regimes. Surface evaporation was shown to have a negligibly small effect on the wave–CISK, which prefers small-scale motion.

The energetics of the EWFB instability is different from that of the wave–CISK. Charney (1971) discussed the energetics of convection in a two-dimensional, conditionally unstable atmosphere ($q > 1$). If the lengths of ascending and descending branches are L_u and L_d, and the average vertical velocities in the ascending and descending areas are W_u and W_d, then the energy generated by upward motion is proportional to $(q-1)W_u^2 L_u$. On the other hand, the energy consumed by downward motion is $W_d^2 L_d$. By using $W_u L_u = W_d L_d$, as is required by mass conservation, the energy generation–consumption ratio is then W_u/W_d or $(q-1)L_d/L_u$. That is, the smaller the ascending area, the more energy can be used to amplify convection. This determines the fate of the wave–CISK, which favors the growth of small-scale disturbances. In a stable atmosphere, however, (A.6) shows that the energy generation rate is proportional to an area integral over the ascending area. Therefore, to generate an EWFB instability, the ascending area cannot shrink to zero but has to be finite. Small ascending and broad descending areas, or small value of L_d/L_u, are a characteristic of the wave–CISK as required by its energetics. For the EWFB instability, however, this is not true since its energetics has nothing to do with the size of the upward velocity, as is obvious in (A.6). In fact, ascending motion occupies half of the equatorial circumference in Fig. 3a.

Recent observations reveal that the tropical atmosphere is marginally stable to deep conditional instability (Xu and Emanuel 1989). The present study confirms that such an atmosphere is unstable. We further show that mean surface easterlies, required in the linear theory (Emanuel 1987; Neelin et al. 1987), are not necessary for the QL-EWFB instability. In fact, zonal-mean surface easterlies appear in our model as a result

of the unstable development of the E mode rather than being its unstable condition. The E mode is very robust. It does not owe its existence to the details of either the heating profile or the stratification. It exists in and dominates the stable parameter regime of the wave–CISK. Furthermore, its phase speed, growth rate, and spatial structure are insensitive to the resolution of the numerical model. These features of the QL E mode suggest that it is an intrinsic mode of the planetary-scale convective motion relevant to the organizing of tropical convection observed in GCMs under the zonally symmetric aqua-planet conditions.

In the R30 GFDL aqua-planet GCM, Hayashi and Golder (1993) find two peaks in the eastward-propagating sector of the zonal velocity power spectrum for wavenumber one, whose typical period ranges are 25–30 and 40–60 days. Although they have different vertical structure and phase speed, the two modes have a similar heating profile. Wave–CISK theory cannot explain this curious double-peak spectrum, since any change in the phase speed of the wave–CISK must result from the change in heating profile (Takahashi 1987). In the stable regime of the wave–CISK, however, a heating can generate two or more neutral baroclinic modes. The inclusion surface evaporation can destabilize them. In the present two-mode model, we have shown that for $f_2 < 0$, there are two EWFB instabilities with the same growth rate and heating profile but with different phase speed and vertical structure. The coexistence of these two EWFB instabilities may explain the double-peaked spectrum found by Hayashi and Golder. Compared with their GCMs, however, the phase speeds of the two EWFB modes with $f_2 = -0.1$ are too fast (corresponding periods are 20 and 26 days, respectively) and the phase speed difference between them is too small.

The E mode can explain the slow eastward propagation and wavenumber one structure of the ISO. At the neutral point of the wave–CISK ($q = 1.0$), its period is 43 days, comparable to the observed. However, its long-lived, concentrated convection spot is unrealistic. In addition, the QL model can deal with only small amplitude convection. When the E mode reaches a large amplitude, the quadratic nonlinearity neglected here will limit its growth and might produce a more realistic spatial structure. In Part II (Xie et al. 1993), we will investigate the nonlinear evolution of the QL-EWFB mode. We will also show that in a fully nonlinear system, eastward-propagating wavenumber one features appear even if the initial stratification is conditionally unstable.

Acknowledgments. We thank Drs. Y. Hayashi, I. Held, Y.-Y. Hayashi, A. Numaguti, and K. Nakajima for helpful discussions. We are grateful to Dr. Y. Hayashi and anonymous reviewers whose comments helped greatly to improve the manuscript. We would like to thank Prof. Y. Toba and other members of Physical Oceanography Group at Tohoku University for their encouragement and discussions. Part of the manuscript was prepared when SPX was at Princeton University as a visiting scientist. He would like to thank Prof. G. Philander for his support and for reading the manuscript.

APPENDIX

An Integral Theorem

By using L, L/C_1, C_1, C_1^2 as characteristic scales of length, time, horizontal velocity, and geopotential, the QL governing equations (3.1)–(3.3) can be written in a nondimensional form

$$\mathbf{u}_t + f\mathbf{k} \times \mathbf{u} = -\nabla\varphi, \tag{A.1}$$

$$\varphi_t + \nabla\cdot\mathbf{u} = (q\nabla\cdot\mathbf{u} + C_E^*\Delta q|\mathbf{u}|)\cdot H(D), \tag{A.2}$$

where $C_E^* = C_E' L$ and $D \equiv \nabla\cdot\mathbf{u}$. Multiplying (A.1) by $\mathbf{u}$ and (A.2) by φ, we obtain an energy equation

$$\frac{1}{2}\frac{\partial}{\partial t}(\mathbf{u}^2 + \varphi^2) = -\nabla\cdot(\mathbf{u}\varphi) + (q\varphi\nabla\cdot\mathbf{u} + C_E^*\Delta q\varphi|\mathbf{u}|)H(D). \tag{A.3}$$

Multiplying (A.2) by $\varphi H(D)$ with the help of $H^2(D) = H(D)$ yields

$$\varphi\nabla\cdot\mathbf{u}H(D) = \frac{1}{1-q} \times \left[-\frac{\partial}{\partial t}\left(\frac{\varphi^2}{2}\right) + C_E^*\Delta q\varphi|\mathbf{u}|\right]H(D). \tag{A.4}$$

Substitution of (A.4) in (A.3) and integrating over the globe yields

$$\frac{\partial}{\partial t}\left\{\frac{\mathbf{u}^2+\varphi^2}{2}\right\} + \frac{q}{1-q}\left\{\frac{\partial}{\partial t}\left(\frac{\varphi^2}{2}\right)H(D)\right\} = \frac{C_E^*\Delta q}{1-q}\{\varphi|\mathbf{u}|H(D)\}, \tag{A.5}$$

where $\{\ \}$ denotes the global mean. For the growing mode solution in (3.4) with an unchanging structure, (A.5) becomes

$$\sigma_i\left\{\mathbf{U}^2 + \phi^2 + \frac{q}{1-q}\phi^2 H(D)\right\} = \frac{C_E^*\Delta q}{1-q}\{\phi|\mathbf{U}|H(D)\}, \tag{A.6}$$

the lhs of which consists of the kinetic potential energies and the energy associated with the moisture process. Note that $\phi^2/2$ is not the available potential energy since the global mean of the geopotential has not been subtracted.

If $C_E^* = 0$, (A.6) gives

$$\sigma_i\left\{\mathbf{U}^2 + \phi^2 + \frac{q}{1-q}\phi^2 H(D)\right\} = 0. \quad \text{(A.7)}$$

For $q < 1$, since every term in the angle bracket of the lhs of (A.7) is positive, σ_i must be zero and there is no growing mode. With $q > 1$, on the other hand, the third term on the lhs of (A.7) becomes negative and a growing mode with $\sigma_i \neq 0$ is possible. This is consistent with the wave–CISK theory.

In a stable atmosphere at rest, since all three kinds of energy are positive with $q < 1$, only surface evaporation can generate a growing mode with a positive σ_i if the rhs of (A.6) is positive. It is obvious that ϕ and hence $\phi|\mathbf{U}|$ are everywhere positive along the equator in a disturbance with the structure shown in Fig. 3. Consequently, the disturbance will be destabilized and grow in amplitude, consistent with our numerical calculation in section 3.

For $q < 1$, the ascending area of an EWFB mode cannot be zero if it is unstable. Otherwise, the rhs of (A.6) will be zero and so is σ_i. In other words, the convective region of an EWFB instability must have a finite size. This distinguishes the EWFB mode from the wave–CISK. By contrast, (A.7) puts no restriction on the size of ascending area of the wave–CISK. Unlike the wave–CISK, the EWFB mode has an upper limit on the growth rate. Using

$$2\{|\mathbf{U}|\phi H(D)\} \leqslant 2\{|\mathbf{U}|\phi\} \leqslant \{\mathbf{U}^2 + \phi^2\} \leqslant \left\{\mathbf{U}^2 + \phi^2 + \frac{q}{1-q}\phi^2 H(D)\right\}$$

for $0 \leqslant q < 1$, we obtain from (A.6)

$$\sigma_i \leqslant \frac{C_E^* \Delta q}{2(1-q)} \equiv \sigma_{\max}, \quad \text{(A.8)}$$

where $\sigma_{\max}$ is the upper limit on the growth rate. The dimensional value of $\sigma_{\max}$ is $(0.54 \text{ day})^{-1}$ for $q = 0.9$ and $\Delta q = 0.2$.

REFERENCES

Bourke, W., 1988: Spectral methods in global climate and prediction models. *Physically-based Modeling and Simulation of Climate and Climatic Change (Part 1)*. M. E. Schlesinger, Ed., Kluwer Academic, 169–222.

Charney, J. G., 1973: Planetary fluid dynamics. *Dynamic Meteorology*, P. Morel, Ed. Reidel.

Dunkerton, T. J., and F. X. Crum, 1991: Scale selection and propagation of wave–CISK with conditional heating. *J. Meteor. Soc. Japan*, **69**, 449–457.

Emanuel, K. A., 1987: An air–sea interaction model of intraseasonal oscillations in the tropics. *J. Atmos. Sci.*, **44**, 2324–2340.

Gill, A. E., 1980: Some simple solutions for heat-induced tropical circulation. *Quart. J. Roy. Meteor. Soc.*, **106**, 447–462.

Hayashi, Y., and D. G. Golder, 1986: Tropical intraseasonal oscillations appearing in a GFDL general circulation model and FGGE data, Part I: Phase propagation. *J. Atmos. Sci.*, **43**, 3058–3067.

—— and ——, 1988: Tropical intraseasonal oscillations appearing in a GFDL general circulation model and FGGE data, Part II: Structure. *J. Atmos. Sci.*, **45**, 3017–3033.

—— and ——, 1993: Tropical 40–50- and 25–30-day oscillations appearing in realistic and idealized GFDL climate models and the ECMWF dataset. *J. Atmos. Sci.*, **50**, 464–494.

Hayashi, Y. Y., and A. Sumi, 1986: The 30–40 day oscillations simulated in an "Aqua Planet" model. *J. Meteor. Soc. Japan*, **64**, 451–467.

Hendon, H. H., 1988: A simple model of the 40–50 day oscillation. *J. Atmos. Sci.*, **45**, 569–584.

Knutson, T. R., and K. M. Weickmann, 1987: 30–60 day atmospheric oscillations: Composite life cycle of convection and circulation anomalies. *Mon. Wea. Rev.*, **115**, 1407–1436.

Kuo, H.-L., 1961: Convection in conditionally unstable atmosphere. *Tellus*, **13**, 441–433.

Lau, K. M., and L. Peng, 1987: Origin of low-frequency (intraseasonal) oscillations in the tropical atmosphere. Part I: Basic theory. *J. Atmos. Sci.*, **44**, 950–972.

Lau, N.-C., and K. M. Lau, 1986: The structure and propagation of intraseasonal oscillations appearing a GFDL general circulation model. *J. Atmos. Sci.*, **43**, 2023–2047.

——, I. M. Held, and J. D. Neelin, 1988: The Madden–Julian oscillation in an idealized general circulation model. *J. Atmos. Sci.*, **45**, 3810–3832.

Madden, R. A., and P. R. Julian, 1972: Description of global-scale circulation cells in the tropics with a 40–50 day period. *J. Atmos. Sci.*, **29**, 1109–1123.

Neelin, J. D., I. M. Held, and K. H. Cook, 1987: Evaporation–wind feedback and low-frequency variability in the tropical atmosphere. *J. Atmos. Sci.*, **44**, 2341–2348.

Numaguti, A., and Y.-Y. Hayashi, 1991: Behaviors of the cumulus activity and the structures of the circulations in the 'aqua-planet' model. Part II: Large scale structures and evaporation–wind feedback. *J. Meteor. Soc. Japan*, **69**, 563–579.

Swinbank, R., T. N. Palmer, and M. K. Davey, 1988: Numerical simulations of the Madden–Julian oscillations. *J. Atmos. Sci.*, **45**, 774–788.

Tokioka, T., K. Yamazaki, A. Kitoh, and T. Ose, 1988: The equatorial 30–60 day oscillation and the Arakawa–Schubert penetrative cumulus parameterization. *J. Meteor. Soc. Japan*, **66**, 883–901.

Wang, B., 1988: Comments on "An air–sea interaction model of intraseasonal oscillation in the tropics." *J. Atmos. Sci.*, **45**, 3521–3525.

Xie, S.-P., 1991: Evaporation–wind feedback and the organizing of tropical convection on the planetary scale: A theory of tropical intraseasonal oscillations. Ph.D. thesis, Tohoku University, Japan, 133 pp + 62 figs.

——, A. Kubokawa, and K. Hanawa, 1993: Evaporation–wind feedback and the organizing of tropical convection on the planetary scale. Part II: Nonlinear evolution. *J. Atmos. Sci.*, **50**, 3884–3893.

Xu, K.-M., and K. A. Emanuel, 1989: Is the tropical atmosphere conditionally unstable? *Mon. Wea. Rev.*, **117**, 1471–1479.